Journal of Alloys and Compounds 504 (2010) 498–502

Contents lists available at ScienceDirect

Journal of Alloys and Compounds

journal homepage: www.elsevier.com/locate/jallcom

Nanostructures and optical properties of hydrothermal synthesized $CeOHCO_3$ and calcined CeO_2 with PVP assistance

C.R. Li[a,b,*], M.Y. Cui[a], Q.T. Sun[a], W.J. Dong[a], Y.Y. Zheng[a], K. Tsukamoto[b], B.Y. Chen[a], W.H. Tang[a]

[a] Department of Physics, Center for Optoelectronics Materials and Devices, Key Laboratory of ATMMT Ministry of Education, Zhejiang Sci-Tech University, Hangzhou 310018, China
[b] Center for Interdisciplinary Research and Graduate School of Science, Tohoku University, Sendai 980-8578, Japan

ARTICLE INFO

Article history:
Received 31 January 2010
Received in revised form 25 May 2010
Accepted 29 May 2010
Available online 11 June 2010

Keywords:
Sphere- or disc-like structures
Hydrothermal method
Polyvinyl pyrrolidone

ABSTRACT

Submicronsized sphere- and disc-like cerium hydroxide carbonate structures were obtained by a hydrothermal method in the presence of polyvinyl pyrrolidone. Morphologies and sizes of the particles and their assembled structures are very sensitive to the concentration of polyvinyl pyrrolidone and the reaction time. As concentration of polyvinyl pyrrolidone increasing or hydrothermal reaction time elongating, the assembled structure experienced a morphology transition from sphere-like to disc-like and then to enlarged sphere-like again. The cerium hydroxide carbonate showed strong photoluminescence effect at room temperature. Ceria nanostructures can be obtained after a 500 °C calcining from cerium hydroxide carbonate precursors. The obtained products showed good ultraviolet absorption properties. Furthermore, the absorbance feature could be adjusted by changing the polyvinyl pyrrolidone concentration and reaction time during synthesis.

1. Introduction

Novel morphologies and sizes controlling of nano/micro materials have attracted much attention due to their special properties and potential applications [1]. Ceria (CeO_2), as a fascinating rare earth material, has shown novel electronic, optical properties and chemical characteristics due to their 4f electrons [2–5]. In order to control the morphologies of ceria-based materials, many methods have been developed. Up to now, different morphologies and sizes of ceria nanoparticles have been synthesized by thermal decomposition of cerium hydroxide carbonate ($CeOHCO_3$) precursors. The morphologies of calcined CeO_2 can normally inherit that of corresponding precursors. For example, prism- [6], dendrite- [7,8] and flower-like [9] $CeOHCO_3$ particles were prepared by the hydrothermal method. Nanocubes and nanospheres of CeO_2 were synthesized by direct thermal decomposition of $Ce(NO_3)_3{\cdot}6H_2O$ in octadecylamine solution [10]. CeO_2 hollow nanospheres were obtained by one-pot [11] and template-assisted [12] hydrothermal approach. Bundle-like, nanorod and octahedron CeO_2 powders were obtained by the precursor pyrolysis [13]. Generally, a series of nanostructures could be achieved by controlling the nucleation, growth, and aggregation of concerned materials. However, the controllable synthesis of nanoparticles in both morphologies and sizes with good physical and chemical properties still remained as a challenge.

In this paper, the assembled $CeOHCO_3$ structure was synthesized by a hydrothermal technique. Effects of the reaction time and surfactant polyvinyl pyrrolidone (PVP) on the morphology and size of as-prepared samples were systematically investigated, and the possible formation mechanism was proposed. The optical properties of the $CeOHCO_3$ and CeO_2 nanoparticles were also investigated.

2. Experimental section

2.1. Synthesis

All chemical reagents used were of analytical grade without further purification. In a typical synthesis process, 2.67 mmol of $CeCl_3{\cdot}7H_2O$ and 0.03 mmol of PVP K30 were dissolved in 15 ml of deionized water under magnetic stirring, and then 0.20 ml of acetic acid and 16.67 mmol of urea were added into the solution. The formed colorless transparent solution was transferred into a 20 ml of Teflon-lined steel autoclave and heated at 180 °C. After the autoclaves were cooled to room temperature, the products were collected by centrifugation, and then washed with deionized water and anhydrous alcohol for three times. The products were dried at 80 °C for 12 h in air, and then calcined at 500 °C for 4 h in air. Finally, straw yellow powder was obtained.

2.2. Characterization

Crystal structures of as-prepared samples were characterized by X-ray diffraction (XRD, the Bruker AXS D8-discover) using Cu $K\alpha_1$ radiation ($\lambda = 0.15405$ nm at 40 kV and 40 mA) in the 2θ range of 10–80°. Fourier transform infrared spectrum was performed on a FTIR, Nicolet Avatar370 using the KBr method. Morphologies and sizes of as-synthesized nanoparticles were studied by field-emission scanning electron microscope (FESEM, Hitachi S-4800). Thermogravimetric analyses were carried

* Corresponding author at: Department of Physics, Center for Optoelectronics Materials and Devices, Key Laboratory of ATMMT Ministry of Education, Zhejiang Sci-Tech University, Hangzhou 310018, China. Tel.: +86 571 86843575; fax: +86 571 86843575.
E-mail address: crli@zstu.edu.cn (C.R. Li).

0925-8388/$ – see front matter © 2010 Elsevier B.V. All rights reserved.
doi:10.1016/j.jallcom.2010.05.151

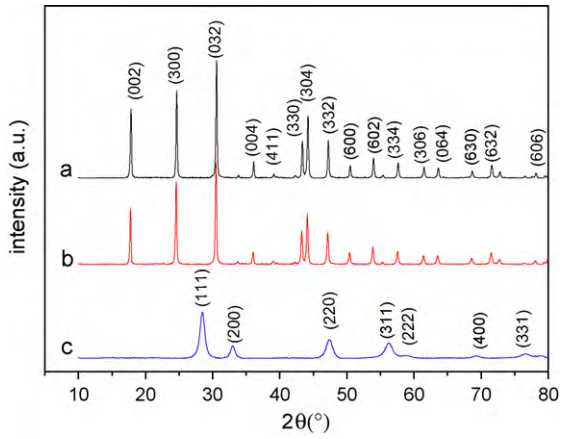

Fig. 1. XRD patterns of the as-synthesized nanoparticles at 180 °C for 3 h (a), 8 h (b) and the calcined sample of (a) at 500 °C for 4 h (c).

out on a TG, PYRIS 1 with a heating rate of 15 °C min^{-1} under flowing air. Photoluminescent (PL) emission spectra were recorded on a fluorescence spectrophotometer (Hitach F-4600) at room temperature (the excitation wavelength is 290 nm). The UV absorption was performed in the range of 200–800 nm on a UNICO UV-4802H UV–vis spectrophotometer.

3. Results and discussion

3.1. XRD characterization

Fig. 1 shows the typical XRD patterns of the samples obtained under hydrothermal reaction at 180 °C for 3 h and 8 h, respectively, along with the sample calcined at 500 °C for 4 h. As shown in Fig. 1a and b, all peaks can be indexed to the pure hexagonal $CeOHCO_3$ structure (P-62c JCPDS No. 32-1089), which indicates a high purity of the hydroxycarbonate. The sharp diffraction peaks in the XRD pattern demonstrated that the products have a good crystallinity. After a heat treatment at 500 °C for 4 h, the hexagonal $CeOHCO_3$ structure was completely converted into cubic CeO_2 structure (Fm3m JCPDS No. 43-1002), as shown in Fig. 1c. The broad diffraction peaks in the XRD pattern of calcined sample indicates that CeO_2 particle grains were refined after the heat treatment.

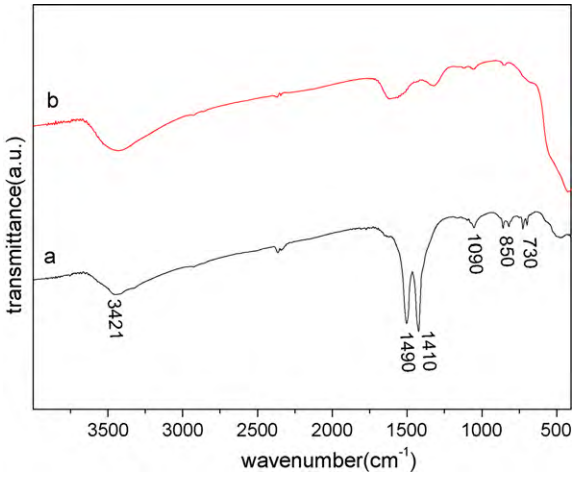

Fig. 2. FTIR spectra of as-synthesized products at 180 °C for 3 h (a) and the calcined products (b).

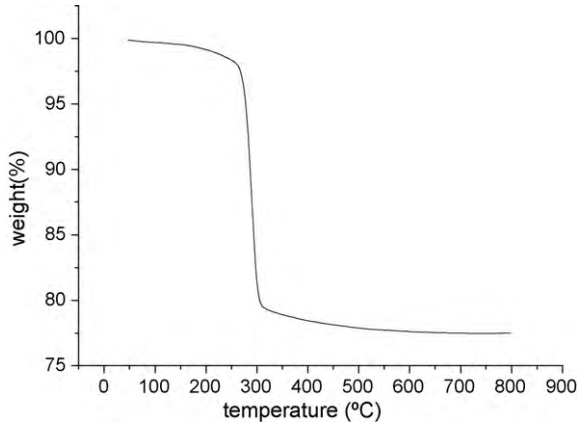

Fig. 3. TG curve of the as-prepared product at 180 °C for 3 h.

3.2. FTIR characterization

Fig. 2 presents the FTIR spectra of the as-synthesized and calcined products. The band centered at 3421 cm^{-1} is ascribed to the O–H stretching vibration in –OH groups. The absorption peaks around 1490 cm^{-1} and 1410 cm^{-1} correspond to the bending vibration of C–H bands and O–C–O stretching, respectively [14]. The bands centered at 1090 cm^{-1}, 850 cm^{-1} and 730 cm^{-1} are attributed to the νC–O, δCO_3^{2-} and $\nu_{as}CO_2$, respectively [15]. The strong broad band below 700 cm^{-1} is assigned to the Ce–O stretching mode [16,17]. After calcination, bands of the residual water or carbonate species become weaker or disappear except for the bands of Ce–O stretching mode [18]. The FTIR results confirmed that the precursor was $CeOHCO_3$ and the CeO_2 was formed after the calcination.

3.3. TG characterization

The thermal stability of $CeOHCO_3$ structure was investigated by TG (Fig. 3). The product started to decompose around 270 °C, and then converted into CeO_2 completely at 500 °C. The main weight loss was about 23% from 270 °C to 500 °C, which agreed with the theoretical value calculated from the decomposition reaction (1):

$$4CeCO_3OH + O_2 \rightarrow 4CeO_2 + 2H_2O + 4CO_2 \quad (1)$$

3.4. SEM characterization

Fig. 4 shows FESEM images of $CeOHCO_3$ structures obtained at 180 °C with different reaction time. After reacting for 1 h, the sphere-like morphology was obtained, which was assembled by ultrafine particles (as seen in Fig. 4a). The morphology of consisting particles was uniform nanosphere with 10–20 nm in diameter (the inset one in Fig. 4a). Similar assembled sphere-like morphology was obtained when reaction time is 2 h, as shown in Fig. 4b, but the consisting particles grew into rod-like shape with non-uniform size (the inset of Fig. 4b). When the reaction time increased to 3 h, the morphology of the aggregated structures was uniform discal shape (Fig. 4c). The average thickness of disc-like particles was about 55 nm, as shown in Fig. 4d. The morphology of consisting particles turned into nanoplate (Fig. 4d). Fig. 4e reveals an assembled disc-like feature with the disc thickness of 133 nm, which was obtained at 180 °C for 6 h. Further, the thickness of the discal particle increased to about 154 nm when the reaction time was elongated to 8 h (Fig. 4f). The morphologies of consisting particles were nanorod structures but with an increment in size as the reaction time was elongated more than 6 h (Fig. 4e and f).

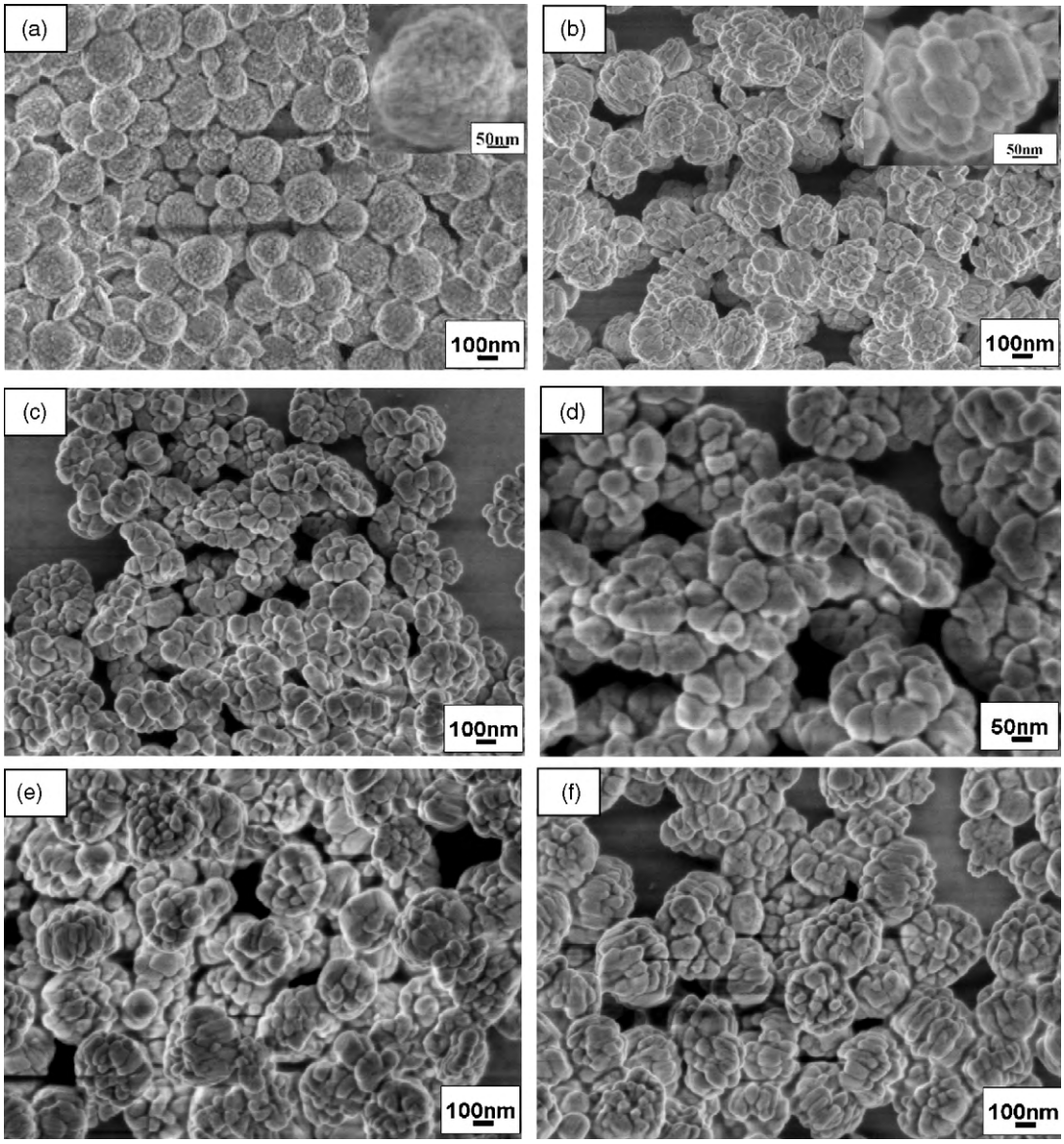

Fig. 4. FESEM images of as-prepared samples at 180 °C for 1 h (a), 2 h (b), 3 h (c, d), 6 h (e), and 8 h (f).

3.5. PVP on the morphology of nanoparticles

To explore the key factor on the formation of assembled nanostructures, effects of the PVP concentration on structures were investigated during the hydrothermal reaction. Without PVP, sphere-like aggregated particles, with an average size of 163 nm, were obtained by reacting for 3 h (Fig. 5a). When 0.017 mmol of PVP was used at the same reaction time, disc-like aggregated particles were obtained and the dimension size in thickness evidentially decreased to about 83 nm (Fig. 5b). The thickness of disc-like particles decreased to 55 nm when 0.03 mmol of PVP was used under the same reaction conditions. On the other hand, when keeping the amount of PVP at 0.017 mmol but elongating the reaction time to 8 h, the thickness of discal particles increased to about 190 nm (Fig. 5c). However, the thickness of aggregated particles reduced to 154 nm when the amount of PVP increased to 0.03 mmol at the reaction time of 8 h.

The effects of PVP amount and hydrothermal reaction time on the particle thickness were summarized in Fig. 5d. It can be clearly seen that the thickness of aggregated particles gradually increases with the reaction time elongating at the same PVP amount, and that decreases as PVP amount increasing at the same reaction time. Therefore, PVP plays an important role on the size and morphology of as-prepared samples.

Effects of PVP on the morphology and size of the aggregated particles can be discussed as following. On the one hand, PVP possesses the structure of a long polyvinyl chain, and it may arise in the steric effect and prevent the particles from aggregation when PVP was absorbed on the surface of $CeOHCO_3$ particle [19]. On the other hand, PVP on the crystal facets of $CeOHCO_3$ changes the relative surface free energies of the facets and may block sites essential to the incorporation of new growth units into the crystal lattice [20]. Consequently, these two effects may change the crystal growth kinetics and then influence on the size and morphology of the particles [21].

3.6. The possible formation mechanism for the disc-like and sphere-like $CeOHCO_3$ structures

The possible formation mechanism of $CeOHCO_3$ nanostructures is proposed schematically in Fig. 6. At the initial stage, ultrafine $CeOHCO_3$ particles in the reaction solution were formed. The formation of $CeOHCO_3$ precursor may experience the following

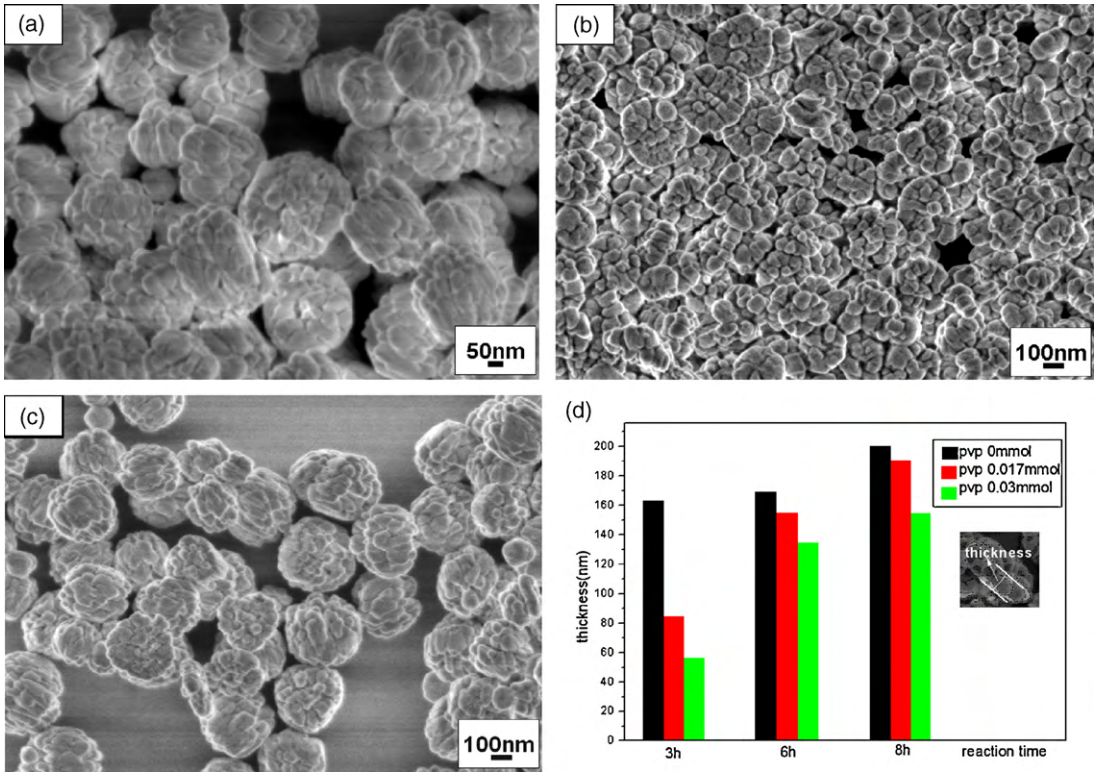

Fig. 5. FESEM images of as-prepared samples at 180 °C: (a) without PVP for 3 h, (b) 0.017 mmol PVP for 3 h, and (c) 0.017 mmol PVP for 8 h, (d) effects of the reaction time and amount of PVP on the thickness of as-prepared samples.

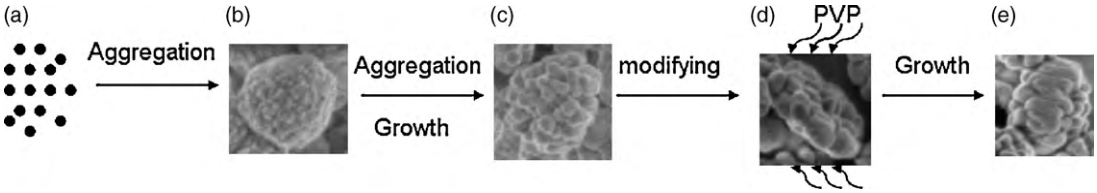

Fig. 6. Schematic depicting possible growth process of disc-like and sphere-like nanoparicles.

reaction process [22]:

$$H_2N\text{–}CO\text{–}NH_2 \Leftrightarrow NH_4^+ + OCN^- \quad (2)$$

$$OCN^- + 2H_2O \rightarrow NH_4^+ + CO_3^{2-} \quad (3)$$

$$Ce^{3+} + yH_2O \rightarrow [Ce(OH)(H_2O)_{n-1}]^{2+} + H_3O^+ \quad (4)$$

$$[Ce(OH)(H_2O)_{n-1}]^{2+} + CO_3^{2-} = CeOHCO_3 + (n-1)H_2O \quad (5)$$

The ultrafine particles in the solution were assembled into nanospheres via oriented attachment (Fig. 6a). To decrease the surface energies, the ultrafine particles of nanosphere aggregated together and grew into larger particles as the reaction time increasing (Fig. 6b and c). After PVP being absorbed on the $CeOHCO_3$ crystal facets, the growth sites of crystal face would be blocked, which may result in a lower growth rate [23]. Finally, the uniform disc-like nanoparticles were obtained (Fig. 6d). As the reaction time was elongated, small particles would grow into large particles, which could reduce the surface free energies, and the sphere-like particles were obtained (Fig. 6e).

3.7. Optical properties of $CeOHCO_3$ and CeO_2 nanoparticles

Fig. 7 shows the PL emission spectra of $CeOHCO_3$ precursors obtained at 180 °C for 3 h, 6 h, and 8 h. The maximum emission occurs at 375 nm with the excitation of 290 nm, which is due to the 5d–4f transitions of Ce^{3+} between the ^2D ($5d^1$) ground state and the $^2F_{5/2}$ ($4f^1$) state [24]. It reveals that the emission intensity will increase with the reaction time increasing. It is well known

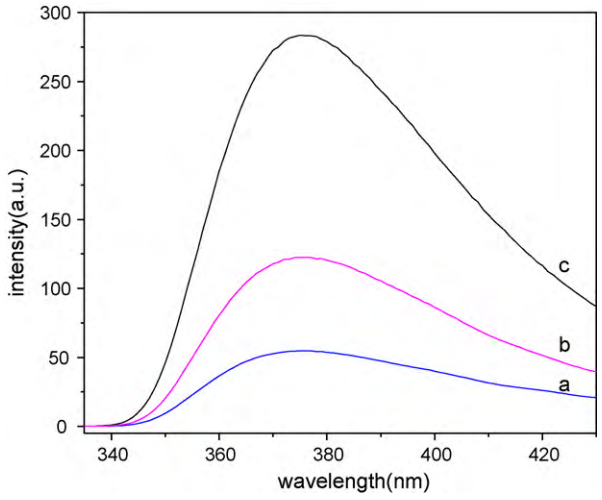

Fig. 7. Luminescent spectrum of as-prepared $CeOHCO_3$ at 180 °C for 3 h (a), 6 h (b), and 8 h (c).

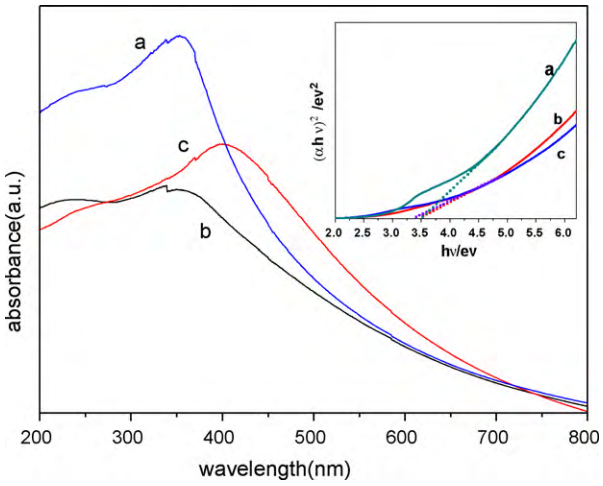

Fig. 8. UV–vis absorption spectra of calcined CeO_2 nanoparticles of which the precursors were prepared at 180 °C for 3 h with different amount of PVP: (a) 0.03 mmol, (b) 0.017 mmol, and (c) 0 mol. The inset is plots of $(\alpha h\nu)^2$ vs photon energy of calcined CeO_2 samples.

that the luminescence properties are related to the morphology and size of the particles [25]. Consequently, they may influence the carriers excited from the valence band to the conduction band and then relax their energy on the crystal surface and lead to variations of luminescence [26]. Different luminescence properties are attributed to the effects of sizes and morphologies of $CeOHCO_3$ particles. Therefore, these materials could be used as black-light materials for pest control [27].

The UV–vis absorption spectra of calcined CeO_2 nanoparticles are shown in Fig. 8. The spectra exhibit strong absorption below 500 nm. It is noted that the absorption of ceria in the UV region originates from the charge-transfer transition between the O^{2-} (2p) and Ce^{4+} (4f) orbit in CeO_2 [14]. The energy band gap of CeO_2 can be obtained from the following equation [28]:

$$\alpha = \frac{K(h\upsilon - E_g)^n}{h\upsilon} \quad (6)$$

where α is the absorption coefficient, K is a constant, E_g is the band gap for direct transitions, and n is 1/2 (direct transitions). The plots of $(\alpha h\nu)^2$ vs photon energy of CeO_2 nanoparticles are shown in the inset of Fig. 8. E_g values of different samples, whose precursors were prepared with 0.03 mmol, 0.017 mmol and 0 mmol of PVP, were determined to be 3.49 eV (Fig. 8a), 3.46 eV (Fig. 8b), and 3.35 eV (Fig. 8c), respectively. These values are larger than that of the bulk materials of 3.19 eV [29,30]. The blue-shifting phenomenon in the UV absorption spectra can be seen clearly. This may be attributed to the decrease of the particle size, and then result in a quantum confinement effect [31].

4. Conclusions

The assembled $CeOHCO_3$ structures have been successfully synthesized by a simple hydrothermal method in the presence of PVP. The disc-like and sphere-like nanostructures can be obtained under different reaction conditions. Similar morphologies of CeO_2 nanostructures to their precursors of $CeOHCO_3$ can be obtained by thermal decomposition at 500 °C for 4 h. Several controlling factors, such as reaction time and concentration of PVP, on the morphology of nanoparticle were systematically investigated. It reveals that PVP is an important factor on controlling the size and morphology of the $CeOHCO_3$ fine particles and their assembled structures. The possible growth process for the assembled structures could be explained by oriented attachment mechanism. The luminescence property indicates that the as-prepared $CeOHCO_3$ nanostructures could be used as black-light materials for pest control. The annealed CeO_2 nanostructures show strong absorption in the UV region. Therefore, CeO_2 nanostructures may be suitable for UV blocking or shielding materials.

Acknowledgments

This work was supported by the National Natural Science Foundation of China (Nos. 10874153, 50772100, and 20701033), Zhejiang National Natural Science Foundation (No. Y407188), Science and Technology Department of Zhejiang Province Foundation (No. 2008C23011).

References

[1] L. Chen, Y. Liu, Z. Lu, D. Zeng, J. Colloid Interface Sci. 295 (2006) 440–444.
[2] D. Esch, F. Esch, S. Fabris, L. Zhou, T. Montin, C. Africh, P. Fornasiero, G. Comelli, R. Rosei, Science 309 (2005) 752–755.
[3] J.V. Herle, M. Horita, J. Am. Ceram. Soc. 80 (1997) 933–940.
[4] S.L. Panayiota, M.E. Angelos, J. Catal. 240 (2006) 182–193.
[5] C. Karunakaran, R. Dhanalakshmi, Sol. Energy Mater. Sol. Cells 92 (2008) 1315–1321.
[6] X.W. Lu, X.Z. Li, F. Chen, C.Y. Ni, Z.G. Chen, J. Alloys Compd. 476 (2009) 958–962.
[7] K. Li, P.S. Zhao, Mater. Res. Bull. 45 (2010) 243–246.
[8] D.E. Zhang, W. Wu, X.Y. Cao, S.Z. Li, X.B. Zhang, G.Q. Han, A.L. Ying, X.Y. Xu, Z.W. Tong, J. Phys. Chem. Solids 70 (2009) 1348–1352.
[9] Z.Y. Guo, F.L. Du, Z.L. Cui, Mater. Chem. Phys. 113 (2009) 53–56.
[10] D.S. Wang, T. Xie, Q. Peng, S.Y. Zhang, J. Chen, Y.D. Li, J. Eur. Chem. 14 (2008) 2507–2513.
[11] Z.J. Yang, L. Liu, H. Liang, H.X. Yang, Y.Z. Yang, J. Cryst. Growth 312 (2010) 426–430.
[12] Z.Y. Guo, F.F. Jian, F.L. Du, Scripta Mater. 61 (2009) 48–51.
[13] M.Y. Cui, J.X. He, N.P. Lu, Y.Y. Zheng, W.J. Dong, W.H. Tang, B.Y. Chen, C.R. Li, Mater. Chem. Phys. 121 (2010) 314–319.
[14] S.F. Wang, F. Gu, C.Z. Li, H.M. Cao, J. Cryst. Growth 307 (2007) 386–394.
[15] C. Sun, J. Sun, G. Xiao, H. Zhang, X. Qiu, H. Li, L. Chen, J. Phys. Chem. B 110 (2006) 13445–13452.
[16] M.L.D. Santos, R.C. Lima, C.S. Riccardi, R.L. Tranquilin, P.R. Bueno, J.A. Varela, E. Longo, Mater. Lett. 62 (2008) 4509–4511.
[17] G.F. Zou, H. Li, D.W. Zhang, K. Xiong, C. Dong, Y.T. Qian, J. Phys. Chem. B 110 (2006) 1632–1637.
[18] M. Jobbagy, F. Marin, B. Schonbrod, G. Baronetti, M. Laborde, Chem. Mater. 18 (2006) 1945–1950.
[19] Z.T. Zhang, B. Zhao, L.M. Hu, J. Solid State Chem. 121 (1996) 105–110.
[20] Q. Li, Z.H. Han, M.W. Shao, X.M. Liu, Y.T. Qian, J. Phys. Chem. Sol. 64 (2003) 295–297.
[21] R.J. Davey, J. Cryst. Growth 34 (1976) 109–119.
[22] H. Masanori, K. Etsuro, J. Am. Ceram. Soc. 82 (1999) 786–788.
[23] R. Si, Y.W. Zhang, L.P. You, C.H. Yan, Angew. Chem. Int. Ed. 44 (2005) 3256–3260.
[24] L.V. Pieterson, M.F. Reid, R.T. Wegh, S. Soverna, A. Meijerink, Phys. Rev. B 65 (2002), 045113-1-16.
[25] D.L. Zhao, Q. Yang, Z.H. Han, J. Zhou, S.B. Xu, F.Y. Sun, Solid State Sci. 10 (2008) 31–39.
[26] Z.H. Han, Y.T. Qian, J. Yang, G.Q. Lu, J. Mater. Chem. 13 (2003) 150–153.
[27] Z.H. Han, Y.T. Qian, K.B. Tang, G.Q. Lu, S.H. Yu, N. Guo, Inorg. Chem. Commun. 6 (2003) 1117–1121.
[28] A. Hartridge, M.G. Krishna, A.K. Bhattacharya, J. Phys. Chem. Solids 59 (1998) 859–866.
[29] Z.Z. Orel, B. Orel, Phys. Status Solidi B 186 (1994) 33–36.
[30] D. Barreca, A. Gasparotto, E. Tondello, C. Sada, S. Polizzi, A. Benedetti, Chem. Vapor Depos. 9 (2003) 199–206.
[31] C.M. Ho, J.C. Yu, K. Tszyan, C.M. Angelo, S. Lai, Chem. Mater. 17 (2005) 4514–4522.